Article

Structural evidence for dimer-interface driven regulation of the type II cysteine desulfurase, SufS

Jack A. Dunkle, Michael Bruno, Franklin Wayne Outten, and Patrick A. Frantom

Biochemistry, **Just Accepted Manuscript** • DOI: 10.1021/acs.biochem.8b01122 • Publication Date (Web): 20 Dec 2018

Structural evidence for dimer-interface driven regulation of the type II cysteine desulfurase, SufS.

Jack A. Dunkle[a]*, Michael Bruno[a], F. Wayne Outten[b] and Patrick A. Frantom[a]*.

[a]Department of Chemistry & Biochemistry, The University of Alabama, Tuscaloosa, AL 35487; [b]Department of Chemistry & Biochemistry, The University of South Carolina, Columbia, SC 29208.

ABSTRACT: SufS is a type II cysteine desulfurase and acts as the initial step in the Suf Fe-S cluster assembly pathway. In *Escherichia coli* this pathway is utilized under conditions of oxidative stress and is resistant to reactive oxygen species. Mechanistically this means SufS must shift between protecting a covalent persulfide intermediate and making it available for transfer to the next protein partner in the pathway, SufE. Here, we report five x-ray crystal structures of SufS including a new structure of SufS containing an inward facing persulfide intermediate on C364. Additional structures of SufS variants with substitutions at the dimer interface show changes in dimer geometry and suggest a conserved β-hairpin structure plays a role in mediating interactions with SufE. These new structures, along with previous HDX-MS and biochemical data identify an interaction network capable of communication between active-sites of the SufS dimer coordinating the shift between desulfurase and transpersulfurase activities.

INTRODUCTION

Cysteine desulfurases are essential enzymes for the mobilization of sulfur into biomolecules including iron-sulfur clusters and modified nucleotides [1, 2]. These 5'-pyridoxal-phosphate (PLP) dependent enzymes use L-cysteine as the sulfur source. An overall mechanism has been proposed for cysteine desulfurases that involves two half reactions: a desulfurase reaction and a transpersulfurase reaction (Scheme 1). In the desulfurase reaction, an external cysteine-aldimine PLP species is initially formed. Abstraction of the α-proton and protonation of the PLP-C4' generates a cysteine-ketimine PLP intermediate. [4-6]. At this stage, an active site cysteine residue (C364 in SufS from *Escherichia coli*, EcSufS) nucleophilically attacks the cysteine sulfur breaking the C-S bond and forming a covalent persulfide intermediate and, following protonation, an alanine-ketimine PLP. After de-protonation of the C4' of the ketimine and re-protonation of the α-carbon, alanine is released with formation of the resting state internal aldimine PLP species. In the transpersulfurase reaction, the covalent persulfide intermediate is transferred

to an active site cysteine residue in an acceptor protein (C51 in SufE) and delivered to its downstream target (Scheme 1). A key mechanistic challenge for these enzymes is the shift between forming the persulfide intermediate in the desulfurase reaction and making it available for transfer to the intended target in the transpersulfurase reaction.

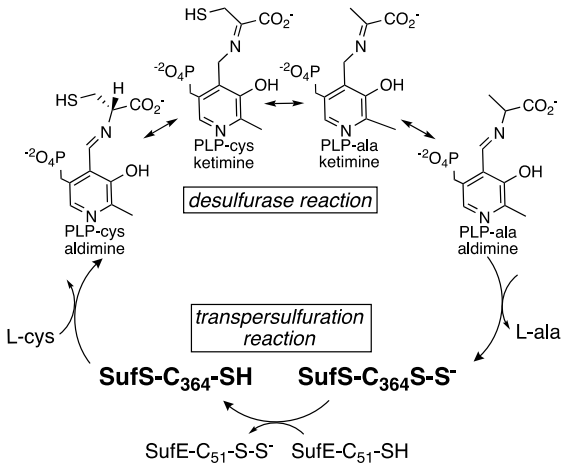

Scheme 1. The two activities of SufS cysteine desulfurases.

Structurally cysteine desulfurases belong to the dimeric aminotransferase V fold and can be categorized as type I and type II enzymes (Figure 1) [2, 7]. The nucleophilic active site cysteine in type I cysteine desulfurases, such as IscS and NifS, resides on a flexible loop containing a twelve-residue insert. Due to this flexibility, the loop is rarely seen in structural reports [8]. When it is seen, the active site cysteine can be up to 23 Å from the PLP cofactor suggesting large conformational changes are necessary for formation of the persulfide intermediate [9]. Consistent with this hypothesis, a recent report suggests the stimulatory role of the accessory protein frataxin is to orient the cysteine-containing loop for proper catalysis in human IscS [10].

In contrast to the type I enzymes, the nucleophilic active site cysteine of type II enzymes resides on a smaller, more rigid loop located ~7 Å from the PLP cofactor [11, 12]. The rigidity of the loop suggests different protein dynamics are involved in controlling the activity of type II enzymes. Indeed, the main challenge in type II enzymes appears to be transfer of the resulting cysteine persulfide intermediate, as specific acceptor proteins are often required to activate type II enzymes [13]. An additional feature of type II enzymes is a 19-residue insertion that forms a β-hairpin motif (residues 254-272 in EcSufS) (Figure 1). The hairpin from one monomer reaches across the dimer interface to interact with the active site on the adjacent monomer. In a previously reported persulfide intermediate structure of EcSufS, the amide of S254 is shown to interact with the persulfide on C364 suggesting the potential for crosstalk between SufS monomers (Figure 2A)[12]. Consistent with this observation, the *N*-terminal base of the β-hairpin, containing S254, has recently been implicated in the proposed "half-sites" regulatory mechanism of SufS in which SufS monomers alternate being active as cysteine desulfurases [3].

Support for the half-sites mechanism comes from biophysical results demonstrating that two equivalents of SufE bind to the SufS dimer with negative cooperativity while activated forms of SufE bind following a one-site model with a

stoichiometry of 0.6-0.7 [14, 15]. Additionally, pre-steady state experiments with SufS from *Bacillus subtilis* show a burst of 0.5 equivalents of alanine produced in the first turnover of the enzyme [16]. Communication between the two active sites is a pre-requisite for a half-sites regulatory mechanism. Results from both backbone amide hydrogen-deuterium exchange mass spectrometry (HDX-MS) on SufS with a covalent persulfide intermediate and site-directed mutagenesis identified a potential communication pathway through a network of charged residues at the dimer interface [3]. Specifically, residues R92, E96, and E250 form cross dimer contacts with R92 capable of interacting with both E96 and E250 from the adjacent monomer (Figure 2A)[11, 12]. It was proposed that the persulfide state of an active site could be communicated to the adjacent monomer via connections between the persulfide intermediate and S254 amide communicated through the dimer interface [3]. Here, we present five SufS x-ray crystal structures which, taken together, confirm a functional role for the dimer interface in mediating long-range conformational changes that affect the orientation of the persulfide intermediate and interactions with SufE.

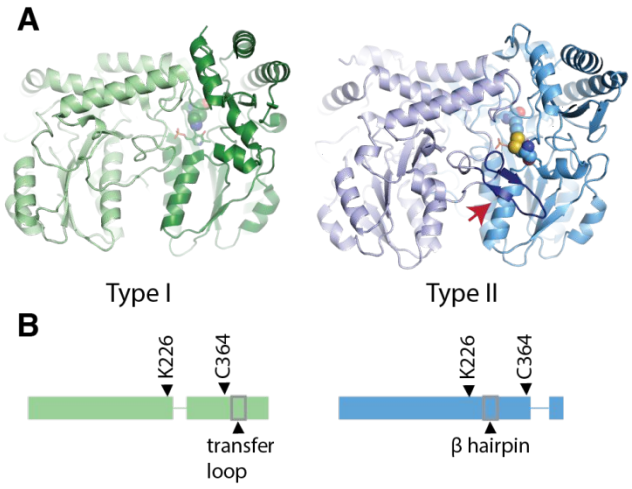

Figure 1. Functionally important sequence insertions define type I versus type II cysteine desulfurases. (A) Type I and type II cysteine desulfurase structures are shown: NifS-like (1eg5, green) and SufS (6mr2, blue). A red arrow marks the β-hairpin unique to type II enzymes. Residues K226 and C364 are shown as spheres. *E. coli* SufS numbers were used to annotate the diagrams. The active site Cys of NifS is not visible because it is disordered in the crystal structure. (B) Type I enzymes lack a β-hairpin structure downstream of the Lys residue that forms an internal aldimine with the 5'-pyridoxal phosphate (PLP) cofactor. Type I enzymes posses an insertion adjacent to the persulfinated Cys residue. Diagrams show the location of the insertions (grey boxes) that define type I versus type II enzymes.

MATERIALS AND METHODS

Generation of SufS Site-Directed Variants

Generation of the dimer interface *E. coli* SufS (UniProt ID P77444) variants (R92A, E96A, and E250A) was previously described [3]. Generation of the H55A SufS variant was accomplished using QuikChange PCR and a *sufS*-containing pET21 plasmid. The following oligonucleotide primer, and its reverse complement, were used to introduce the mutation: 5'-GGCTACGCGGCGGTGGCTCGTGGTATTCATAC-3'. The resulting plasmid was transformed into XL-10 Gold *E. coli* cells.

Purified plasmid was sent for DNA sequencing (Eurofins, Louisville, KY) to ensure the desired mutation had been incorporated.

Protein Expression and Purification

SufS and SufS variants were purified as previously reported [17]. Briefly, a pET21 plasmid containing the mutated *sufS* gene was transformed into Δ*sufS* BL21(DE3) *E. coli* cells for recombinant expression. Cells were grown at 37 °C and protein expression was induced after cells reached an O.D. of 0.6 using 0.5 mM isopropyl-β-D-thiogalactoside (IPTG). After 4 hours of post-induction growth, cells were pelleted and stored at -20 °C. Cells were lysed via sonication and the clarified lysate was subjected to FPLC chromatography in the following order: HiTrap Q HP, HiTrap Phenyl HP, and Superdex200 (all chromatography materials from GE Healthcare). Fractions from each chromatographic step were analyzed by SDS-PAGE and only fractions containing SufS were used in the subsequent step. For long-term storage, 10% glycerol was added and purified protein was stored at -20 °C. To verify that SufS variants retained the quaternary structure of wild-type SufS, size-exclusion chromatography was performed. Approximately 600 - 800 μg of each protein was loaded to a Superdex S200 10/300 column and chromatography was performed in a 50 mM 3-(*N*-morpholino)propanesulfonic acid (MOPS) pH 7.4, 150 mM NaCl and 10 mM 2-mercaptoethanol buffer.

SufS Alanine-Detection Assay

L-Alanine production by H55A SufS was determined using a high-throughput fluorometric assay previously developed in the Dos Santos lab [18]. The assay contained the following components: 0.4 uM SufS, 100 mM MOPS, pH 8.0, 2 mM tris(2-carboxyethyl)-phosphine hydrochloride (TCEP), and varying amounts of SufE and L-cysteine. A 500 uL reaction was initiated by the addition of SufS and quenched at various times (0, 3, 6, and 9 minutes) using 5 uL of 10% TCA. L-Alanine production was determined by addition of 200 uL of a detection buffer (115 mM sodium borate, pH 9.0, 6 mM potassium cyanide, and 0.61 mM 2,3-naphthalenedicarboxaldehyde). This mixture was allowed to develop in the dark for 20 mins. After this incubation period, 150 uL was transferred to a 96-well plate and fluorescence was measured (excitation 390 nm/emission 440 nm) using a Biotek Synergy2 multi-well plate reader. A standard curve of L-alanine was prepared under the same experimental conditions. The standard curve was used to convert fluorescence intensity to nmoles L-alanine and progress curves of L-alanine production by SufS were constructed. Initial velocities at various substrate concentrations from this analysis were fit to the Michaelis-Menten equation to determine kinetic parameters.

Crystallization and X-ray Structure Solution

SufS variants at 6-13 mg/mL were mixed with crystallization solution (4-4.5 M NaCl, 0.1 M MES pH6.5) in a ratio of 1 μL protein to 2 μL crystallization solution [12]. Targeted crystallization screens were performed at 20°C using the sitting drop method around the conditions previously reported with 4 – 4.5 M NaCl as the precipitant [12]. Each SufS variant formed single crystals in less than 7 days. Prior to x-ray data collection, crystals were cryo-protected in mother liquor mixed with 50-100% glycerol in a 1:1 ratio and flash frozen in liquid N_2. X-ray data collection was carried out at the Advanced Photon Source beamline 22-ID outfitted with an Eiger 16M detector using 0.5° oscillations and a 1.000 Å wavelength. Reflections were integrated and merged using XDS except for the H55A and E96A datasets where HKL2000 was used [19, 20]. Phases were obtained by molecular replacement using Phaser within the PHENIX software suite and 1jf9 as a search model with all heteroatoms removed [12, 21]. Initial structure solutions were refined in PHENIX. Manual model building was performed in Coot and iterative cycles of model building and refinement were performed including individual sites and individual atomic displacement parameter (ADP) refinement. Occupancy of the persulfide S atom was refined once ADP values had converged to produce the final models [22]. Restraints for the 5'-pyridoxal phosphate cofactor were obtained from RCSB Ligand Expo and applied during refinement. X-ray data statistics and model quality data are reported in Table 1. Figures were made with Pymol [23].

Anomalous Diffraction

High multiplicity, low dose x-ray diffraction data was collected using 1.740 Å wavelengths at beamline 22-ID of the Advanced Photon Source following published strategies [24, 25]. Using 1.2% transmission, two 360° sweeps were made with oscillations of 0.25° per image and 0.25 seconds exposure time on a SufS wt crystal. An additional 360° sweep was collected on a second SufS wt crystal with the same data collection strategy. The data from both crystals was integrated with XDS and merged with XSCALE once identified as isomorphous [19]. The combined dataset possesses anomalous signal by the $CC_{1/2}$ criterion to 3.59 Å (Table 1) [26]. Since this data was also isomorphous with the native SufS wt diffraction data, fourier synthesis was used to generate the anomalous maps shown in Figure 3. As an additional test to verify the presence of the C364 persulfide, the Phaser-EP and Autosol modules in PHENIX were used to identify heavy atom sites and the persulfide sulfur and the C364 sulfur were successfully located [21].

Sequence Conservation Analysis

To analyze the conservation of residues in the dimer interaction network, a sequence similarity network (SSN) was constructed from the IPR010970 Interpro family (18,567 sequences) [27]. Sequences were binned into representative nodes if their alignment score was 45 or better creating 1011 representative nodes. The online EFI-EST tool was used to create the .xgmml file for

import into Cytoscape. 29 nodes with >100 sequences were identified [28, 29]. A representative sequence from each repnode was selected for use in a multiple sequence alignment with preference given to Swiss-Prot reviewed entries. A SSN network with edges connecting nodes if their alignment scores were 140 or better shows the selected nodes are well distributed across the network. MUSCLE was used for alignment of the 29 representative sequences and Protskin was used to map conservation scores to the SufS coordinates [30, 31].

RESULTS

Table 1 | Data collection and refinement statistics

	wt 6MR2		**H55A 6MR6**	**R92A 6MRE**	**E96A 6MRH**	**E250A 6MRI**
	Native	Anomalous				
Data collection	APS 22-ID	APS 22-ID	APS 22-ID	APS 22-ID	APS 22-ID	APS 22-ID
Space group	$P4_32_12$	$P4_32_12$	$P4_32_12$	$P4_32_12$	$P4_32_12$	$P4_32_12$
Cell dimensions						
a, b, c (Å)	127.03, 127.03, 134.49	127.11, 127.11, 134.23	127.01, 127.01, 133.68	126.98, 126.98, 135.22	125.97, 125.97, 136.95	125.73, 125.73, 138.55
α, β, γ (°)	90, 90, 90	90,90,90	90, 90, 90	90, 90, 90	90, 90, 90	90, 90, 90
Wavelength	1.000	1.74	1.000	1.000	1.000	1.000
Resolution (Å)[a]	92.35-2.40 (2.54-2.40)	92.29-3.59 (3.68-3.59)	44.91 - 2.01 (2.09 - 2.01)	92.56 - 2.50 (2.56 - 2.50)	43.5 - 2.01 (2.09 - 2.01)	93.10 - 2.62 (2.71 - 2.62)
R_{meas} (%)	12.6 (120.0)	9.3 (15.3)	13.6 (123.1)	15.6 (163.6)	10.4 (151.6)	16.9 (75.7)
I/σI	10.94 (1.38)	45.82 (31.61)	22.25 (1.39)	15.97 (2.09)	28.57 (1.01)	6.79 (2.09)
Completeness (%)	99.6 (97.7)	100.0 (100.0)	96.5 (97.2)	99.9 (99.9)	99.4 (90.5)	92.4 (94.9)
Redundancy	6.97 (6.97)	40.82 (41.32)	6.3 (6.0)	12.7 (12.0)	7.6 (7.0)	7.0 (7.39)
$CC_{1/2}$ (%)	99.7 (64.6)	99.9 (99.8)	99.4(59.9)	99.8 (68.3)	99.9 (49.7)	98.9 (59.2)
Refinement						
Resolution (Å)	40.11 - 2.40 (2.49 - 2.40)		44.91 - 2.01 (2.09 - 2.01)	42.61 - 2.5 (2.58 - 2.50)	43.50 - 2.01 (2.09 - 2.01)	60.67 - 2.62 (2.71 - 2.62)
No. reflections	43,227 (4,120)		69,571 (6,899)	38,826 (3,813)	72,510 (7,029)	31,343 (3,118)
R_{work}/R_{free} (%)	16.83 (28.28) / 19.06 (31.95)		18.67 (28.24) / 20.19 (26.82)	17.80 (29.46) / 19.87 (32.19)	19.48 (28.10) / 21.20 (28.91)	18.45 (26.70) / 21.63 (30.35)
No. atoms	3,256		3,274	3,269	3,251	3,215
Protein	3,119		3,114	3,113	3,115	3,115
Ligand	16		16	16	16	16
Water	121		144	141	120	84
B factors						
Protein	54.68		30.97	55.03	40.34	53.48
Ligand	50.60		27.28	47.72	35.63	51.24
Water	57.61		33.32	60.40	42.31	56.83
R.m.s deviations						
Bond lengths (Å)	0.008		0.007	0.008	0.007	0.008
Bond angles (°)	0.94		0.87	0.97	0.95	0.95

[a] Values in parentheses are for the highest-resolution shell

Wild-type SufS and variant SufS enzymes containing alanine substitutions at positions R92, E96, E250 and H55 were expressed and purified as previously described [17]. Cysteine desulfurases possess a homodimeric quaternary structure [2]. Therefore the quaternary structure of each point mutant residing at the dimer interface (R92A, E96A, E250A) was analyzed by size exclusion chromatography indicating each retained a homodimeric structure (Figure S1). Each SufS variant readily formed single crystals typically diffracting x-rays to 2.0-2.7 Å resolution with the 2-fold symmetry axis of the crystal producing a C2 symmetric SufS homodimer in both wild-type and mutant SufS structures (Table 1). In a previous crystal structure, the SufS homodimer was also observed to reside on a two-fold crystallographic symmetry axis [12]. As previously reported, SufS residues R92, E96 and E250 form an extensive network of electrostatic interactions at the dimer interface (Figure 2A) [3]. The E96A and E250A enzyme variants have an altered Michaelis constant (K_{SufE}) and, now x-ray data reveal, altered dimer geometries (Figure 2, Table 2). Superimposing the wild-type dimer and SufS E96A or E250A dimer via monomer A reveals a rotation of approximately 3.5° with the axis of rotation nearly parallel to the R92-E96 salt bridge (Figure 2C, 2D). The change in dimer geometry in the E96A and E250A variants correlates with structural changes at the dimer interface that disrupt the salt bridge leading to elevated crystallographic atomic displacement parameter (B-factor) values and suggest it can act as a hinge region (Figures 2C, 2D, S2). Inspection of the dimer interface of the E96A or E250A mutant reveals new hydrogen bonding interactions occur that offset the loss of the electrostatic interactions and drive dimer rearrangement (Figure S3). Loss of either binding partner is sufficient to shift the side chain of R92 ~3 Å such that it now is directed towards I233'. Importantly, in both the E96A and E250A variants the re-organized dimer interface leads to the residues 255-271 β-hairpin to pivot away from the active site (Figure 2C, 2D). The pivot, which is most pronounced in the SufS E250A variant, is ~2 Å in magnitude. While this change is modest, the base of the β-hairpin of each SufS monomer lies at ~ 4 Å distance from the C364 in the adjacent monomer. This proximity suggests that perturbation of the dimer geometry in E96A and E250A SufS may explain the decrease seen in the k_{cat}/K_M term for SufE in steady state assays for those mutant proteins (Figure 2, Table 2).

Table 2. Kinetic Parameters for Wild-Type and SufS Variants[a]

SufS	k_{cat} (min^{-1})	K_{Cys} (μM)	k_{cat}/K_{Cys} (μM^{-1} min^{-1})	K_{SufE} (μM)	k_{cat}/K_{SufE} (μM^{-1} min^{-1})
WT	12.1 ± 0.4	50 ± 7	0.24 ± 0.003	0.41 ± 0.05	30 ± 4
H55A	39 ± 3	75 ± 15	0.5 ± 0.1	0.73 ± 0.07	100 ± 12
R92A	7.4 ± 0.2	95 ± 10	0.08 ± 0.01	0.63 ± 0.09	12 ± 2
E96A	13.8 ± 0.6	95 ± 10	0.14 ± 0.02	2.6 ± 0.3	5.3 ± 0.7
E250A	10.0 ± 0.4	81 ± 9	0.12 ± 0.01	2.4 ± 0.2	4.1 ± 0.4

a. WT, R92A, E96A, E250A previously reported in Kim *et al.* [3].

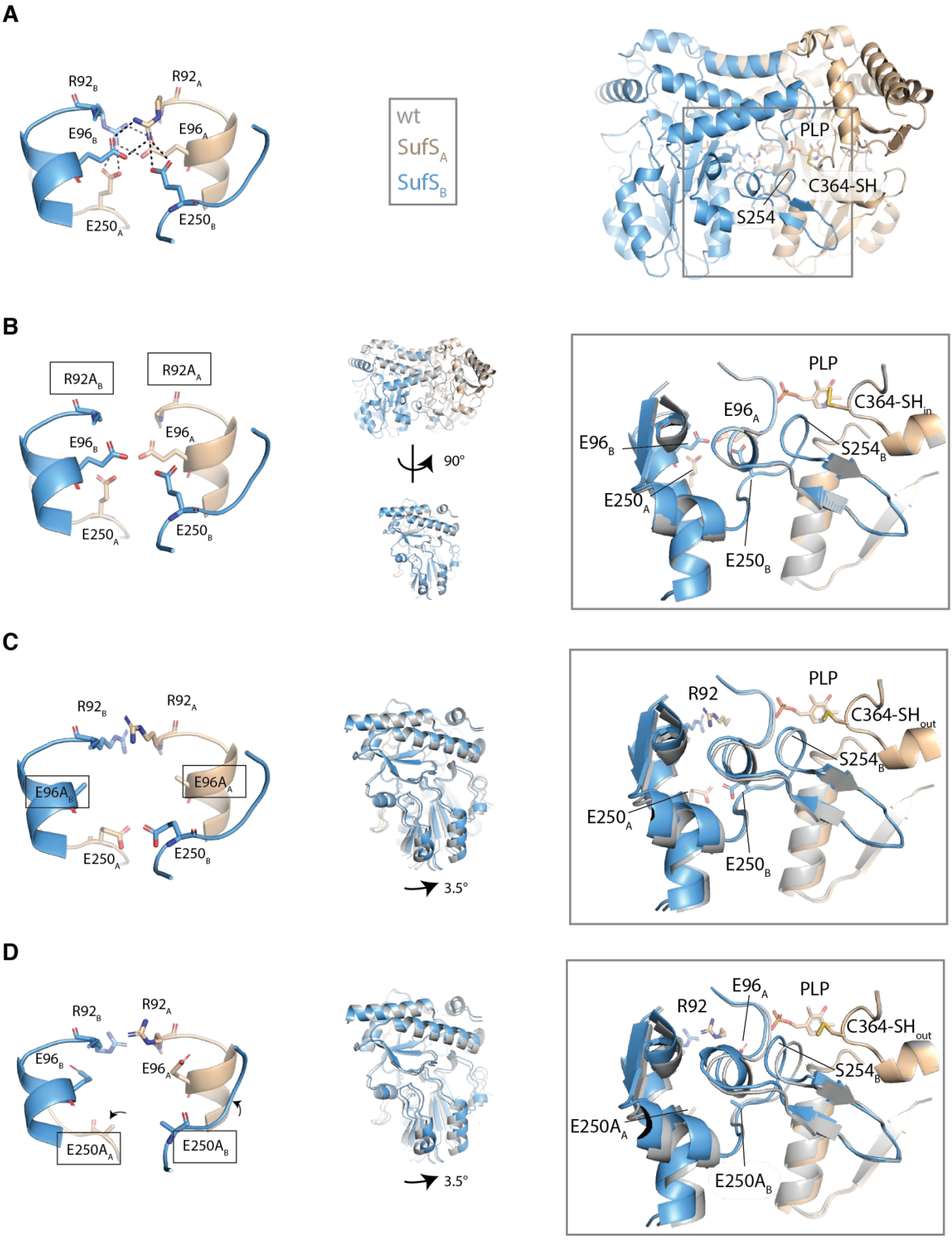
A
R92B
R92A
E96B
E96A
E250A
E250B
wt
SufSA
SufSB
PLP
C364-SH
S254
B
R92AB
R92AA
E96B
E96A
E250A
E250B
90°
PLP
E96A
C364-SHin
E96B
S254B
E250A
E250B
C
R92B
R92A
E96AB
E96AA
E250A
E250B
3.5°
R92
PLP
C364-SHout
S254B
E250A
E250B
D
R92B
R92A
E96B
E96A
E250AA
E250AB
3.5°
E96A
R92
PLP
C364-SHout
S254B
E250AA
E250AB

Figure 2. Electrostatic interactions at the SufS dimer interface control the active site conformation. (A) Details of the SufS dimer interface are shown along with an overview of the dimer. PLP and C364 mark the enzyme's active site. A grey box indicates the region shown in close-up images below. SufS monomer A is colored in tan and SufS monomer B is colored in blue. (B) A detailed view of the dimer interface is shown revealing that the R92A mutant causes loss of the electrostatic interactions at the interface, however, a superposition of SufS R92A (blue and tan) with wild-type (wt) SufS (grey) reveals the mutant does not cause global changes to the dimer's structure. (C) The E96A mutant causes a loss of the electrostatic interactions at the dimer interface and a re-organization of the dimer juxtaposition such that monomer B is rotated by 3.5° relative to its wt orientation. The dimer interface change causes a small movement of the residue 255-271 β-hairpin. (D) The SufS E250A mutant possesses a loss of dimer electrostatic interactions, monomer B rotation and a pivot of the residue 255-271 β-hairpin away from the monomer A active site.

In contrast, the SufS R92A mutant, which displays a 2.5 to 3-fold decrease in k_{cat}/K_M values for both substrates, shows dimer geometry identical to that seen in the wild-type structure with the positions of E96 and E250 undisturbed (Figure 2B, Table 2). The x-ray structure offers an explanation for the contradiction: difference electron density maps of the SufS R92A mutant reveal positive peaks in the region left vacant by the absence of the Arg guanidinium group which may indicate Na^+ or a similar positive ion is able to substitute for the interactions of the Arg sidechain in the crystal (Figures S4). However, the relevance of this observation to the kinetic defects of the R92A variant is unclear since the crystallization was carried out in a non-physiological, ~4 M concentration of Na^+.

Inspection of the active site in all four structures revealed the presence of extra density adjacent to the sulfur atom of C364, the nucleophilic cysteine residue in SufS (Figure 3A). This density is best modeled as a covalent persulfide intermediate in the monomeric asymmetric unit. In R92A and E96A SufS, the persulfide was estimated to be ~80%, with wild-type and E96A SufS having ~60% crystallographic occupancy (Table 3). The enzymes had not been in the presence of exogenous cysteine subsequent to their purification suggesting the persulfide was part of the 'as-isolated' protein. To confirm that the additional density was indeed due to the persulfide, a sulfur anomalous diffraction experiment was performed to directly detect the presence of the sulfur atoms (Table 1). To address equipment limitations and the tradeoffs between x-ray absorption, radiation damage and anomalous signal magnitude, a high redundancy, low-dose dataset was collected on a SufS wild-type crystal with 1.74 Å wavelength synchrotron x-rays (Table 1) [24, 25]. The resulting anomalous map shows peaks at 3 σ for the phosphate of PLP and peaks for sulfur atoms of many Met and Cys residues throughout SufS confirming map quality (Figure 3B, 3C). An anomalous peak at C364 confirms the presence of the persulfide enzyme intermediate (Figure 3B). Additionally, using combined phase information from the anomalous data and molecular replacement, PHENIX AutoSol software placed sulfur atoms in the location of the persulfide [21]. Several anomalous peaks are present at locations indicative of solvent ions including

Table 3. Crystallographic Occupancy of SufS C364 Persulfide

SufS Variant	Occupancy
wt	0.63
H55A	0.66
E96A	0.80
R92A	0.84
E250A	0.63

two peaks in the active site (Figure 3B). These peaks may be attributable to chloride since chloride is present at ~ 4M during crystallization and has an x-ray absorption edge near sulfur.

Structures of both wild-type and R92A SufS show the persulfide in a new position, pointed into the active site (Figure 3D). In contrast, the persulfide found in E96A and E250A SufS points out of the active site in a manner similar to the previously reported persulfide intermediate SufS structure (Figure 3D) [12]. Superposition of the wild-type structure with a previously reported structure containing an external aldimine analog shows the persulfide is positioned appropriately at 3.4 Å from the β-carbon position the persulfide is expected to occupy immediately following sulfur transfer (Figure 3E) [7]. Based on its positioning we believe the inward facing conformation of C364 is an earlier intermediate in the SufS reaction, after the desulfuration of L-cysteine has occurred but prior to full transition to the transpersulfuration step.

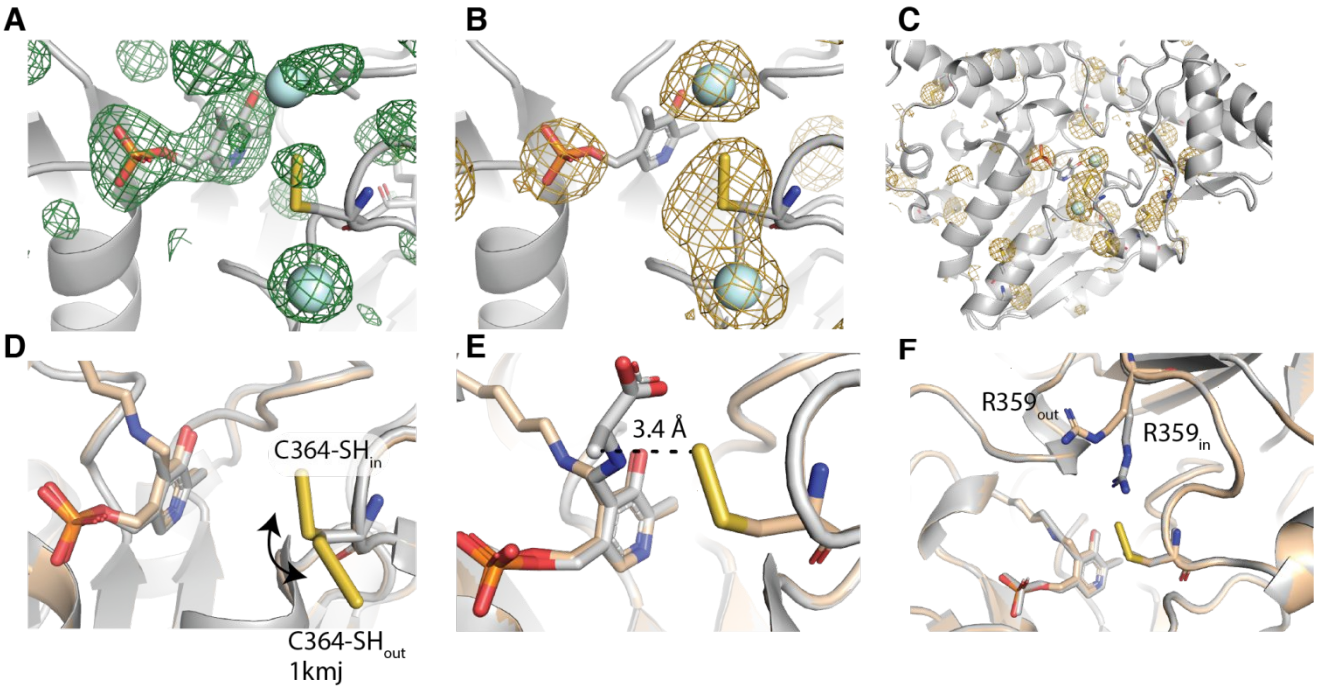

Figure 3. C364 persulfide observed in the "in" conformation**.** (A) Positive peaks (green) in an unbiased, F_o - F_c difference electron density map contoured at 3σ reveal density for PLP, solvent ions and C364 persulfide. (B) An anomalous difference map, contoured at 3σ, of the SufS active site. In addition to the phosphate and persulfide peaks, additional peaks appear which may result from chloride in the crystallization conditions. (C) An anomalous difference map, contoured at 3σ, showing sulfur peaks at Met and Cys residues throughout SufS. (D) A superposition of C364 persulfide wt SufS (this work, 6mr2) and structure 1kmj which contained persulfide Cys 364 in an 'out' orientation. (E) A superposition of C364 persulfide wt SufS (6mr2) and structure 1i29 containing an external aldimine intermediate reveals the "in" persulfide is positioned 3.4 Å away from C_β as expected immediately following sulftur transfer. (F) Wt SufS (6mr2) and 1jf9 are superpositioned to reveal alternate positions of R359 which may control access of the substrate to the active site.

Two other changes are seen in the active sites of these structures relative to the previously reported wild-type structure. In all four structures, R359 moves out of the active site (Figure 3F). This is similar to the shift from the previously reported

persulfide intermediate structure [12]. Additionally, a change in position in H55 can been seen in the E250A SufS structure (Figure 4A, 4B). In the wild-type SufS structure, H55 interacts with S254 on the β-hairpin motif (Figure 4A). In the E250A structure, the imidazole ring moves 2.5 Å towards the active site placing it ~3.5 Å from the inward-facing persulfide (Figure 4B). This led us to hypothesize that H55 may play a role in catalysis or regulation of SufS. An H55A variant of SufS was previously reported as having no effect on SufS activity [7]. However, this experiment was performed in the absence of SufE. We performed a steady-state kinetics analysis of SufS H55A in the presence of SufE and solved its x-ray crystal structure (Tables 1, 2). Kinetic characterization of H55A SufS revealed a k_{cat}/K_M approximately two-fold larger than wild-type enzyme for cysteine and approximately three-fold larger for SufE. The origin of this rate increase is not clear. An x-ray structure of the variant was superimposable with the wild-type structure except at the precise location of the substitution (Table 1, Figure 4C). Together these results suggest that H55 is dispensable for SufS catalysis and regulation.

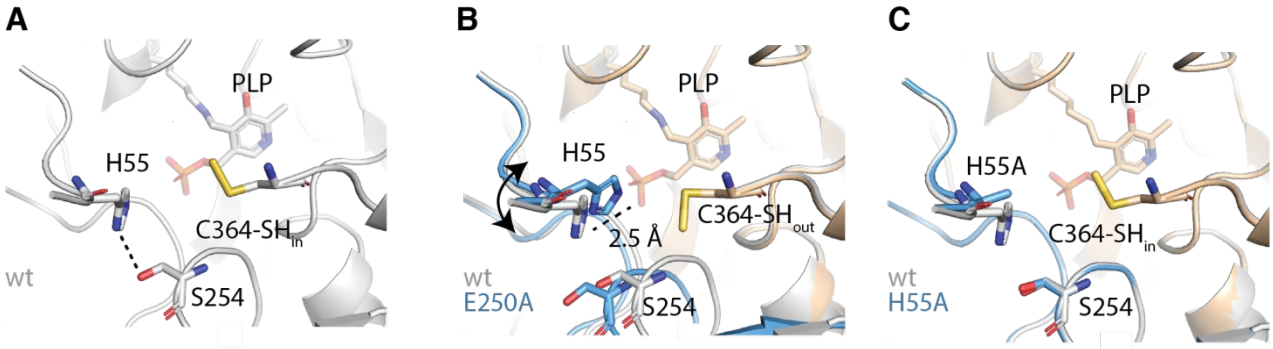

Figure 4. The active-site H55 residue is dispensable for function. (A) H55 can hydrogen-bond to S254 suggesting a role in active site dynamics. (B) The H55-S254 hydrogen-bond is broken in the SufS E250A structure allowing H55 to move towards the C364 persulfide. (C) The structure of the SufS H55A mutant does not cause broader structural changes in the active site.

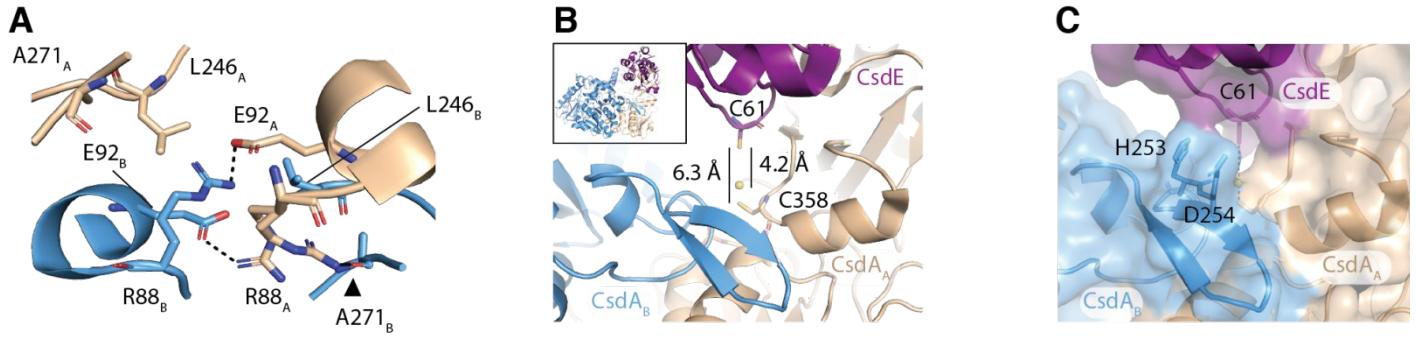

Figure 5. The crystal structure of CsdA-CsdE indicates it possesses an interaction network that may coordinate its cysteine desulfurase and sulfur transfer activities. (A) A structural alignment of SufS with CsdA indicates that dimer interface residues R92, E96 and E250 of SufS correspond to R88, E92 and L246 of CsdA. $R88_A$ is modeled in two alternative conformations in crystal structure 4l4w. The R88-E92 interaction is very similar to that seen in SufS between R92 and E96 but in the absence of a residue homologous to SufE E250, R88 can form a H-bond to the carbonyl of A271 (arrow). (B) C61 of CsdE is positioned 6.3 Å from the C358 thiol. If a persulfide is modeled onto C358, C61 at 4.2 Å is still too far away for sulfur transfer indicating an additional conformational change must occur to promote the reaction. (C) A surface rendering of CsdA-CsdE indicates the β hairpin is sterically blocking a closer approach of C61 to C358.

Since the β-hairpin formed by residues 255-271 of SufS is a conserved feature of type II cysteine desulfurases we considered whether the structural changes at the dimer interface affecting S254 and the β-hairpin might influence the interaction between SufS and SufE during transpersulfuration [2]. No crystal structure of SufS bound to SufE exists, however, *E. coli* CsdA possesses 43% sequence identity to *E. coli* SufS, so the crystal structure of CsdA bound to CsdE, a SufE homolog, is useful for examining the role of the β-hairpin [32]. Several details of the $CsdA_2$-$CsdE_2$ crystal structure (4lw4) are consistent with the hypothesis that structural changes at the dimer interface affect CsdA function [32]. In the $CsdA_2$-$CsdE_2$ crystal structure, two different orientations of CsdE are observed, one in which the C61 transpersulfuration substrate is positioned into the active site of a CsdA and one in which it is not. This supports the idea that the cysteine desulfurase may only engage productively with one transpersulfuration substrate at a time. $CsdA_2$-$CsdE_2$ does not possess perfect symmetry between the CsdA proteins and one of the regions where symmetry is broken is the dimer interface. The salt bridge equivalent to SufS R92 – E96 is conserved in CsdA (Figure 5A) and interestingly CsdA R88, the SufS R92 equivalent, is modeled in two alternative conformations indicating it is dynamic. In addition to the conformation that interacts with E92, R88 is seen forming a H-bond to the carbonyl of A271, which sits at the C-terminus of the β-hairpin structure (Figure 5A). The structure indicates R88 can alternate between its interaction with E92, which if it behaves similarly to the EcSufS crystal structures, would promote β-hairpin movement, and its interaction with A271 which may restrict β-hairpin movement. Inspection of the manner in which CsdE chain C is inserted into the CsdA active site reveals that while it makes a close approach to C358 at 6.3 Å, C61 is still too far away for sulfur transfer (Figure 5B). Modeling C358 as a persulfide reveals that the labile sulfur would still be located 4.3 Å from CsdE C61. Since this

distance is still too far for sulfur transfer an additional conformational change must be necessary for the reaction to occur (Figure 5B). A surface rendering of CsdE and the CsdA β-hairpin reveals that it is sterically blocking a closer approach of C61 into the active site (Figure 5C). Therefore the crystal structure of CsdA-CsdE reveals that a movement of the β-hairpin, similar in magnitude and direction to that observed in the SufS mutants, is necessary for catalysis. The CsdA-CsdE crystal structure also reveals an interaction network, similar to that in SufS, exists which may modulate β-hairpin dynamics.

DISCUSSION

Previous HDX-MS identified four peptides whose dynamics changed when SufS was probed in the resting versus the C364 persulfide state [3]. These included peptides covering active site residues, 225-236 and 356-366, and peptides covering the dimer interface, 88-100 and 243-255 (Figure 6A). Changes in the two active site regions had previously been identified by HDX-MS when SufE or an activated variant of SufE (D74R SufE) bound to SufS [14, 15]. HDX-MS results with the activated D74R SufE also indicated changes in peptide 88-100, suggesting that the dimer interface is sensitive to activated intermediates in the SufS/SufE reaction. What was unclear was whether or not the HDX-MS signals represented a coordinated conformational change involving both the dimer interface and the active site. Based on structures of wild-type SufS it was observed that all four peptides identified in the SufS persulfide HDX-MS study were adjacent in the atomic coordinates [11, 12]. Additionally, a link was postulated between the dimer interface peptides based on the observation of the R92-E250 electrostatic interaction. It was proposed that since the amide backbone of S254 had been observed to hydrogen bond to C364 persulfide on the adjacent monomer, changes in the position of E250 could propagate to S254 and then to the active site of the adjacent monomer providing a potential mechanism for the proposed half-sites regulation[3]. However, an important discrepancy existed: the crystal structures of apo SufS versus SufS persulfide revealed no difference between the coordinates outside of the small local changes at C364 and R359 [12]. This could be explained by the fact that HDX-MS is performed on the protein in-solution and that the persulfide in the previously reported structure was formed by incubation of the pre-formed crystals with cysteine [12]. Nevertheless, there was no crystal structure data that supported coordinated conformational changes between the dimer interface and active site.

The HDX-MS data, indicating structural changes were associated with SufS persulfide formation, were investigated further by site-directed mutants that disrupted the electrostatic interactions between R92 and E96 or R92 and E250 [3]. Size exclusion chromatography showed that point mutants of the interface residues still formed dimers and steady-state kinetics data showed that k_{cat}/K_{Cys} was only mildly affected (Figure S1, Table 2) [3]. k_{cat}/K_{SufE}, however, decreased in the E96A and E250A

mutants indicating a disruption of the SufS-E interaction (Table 2) [3]. This was the first data that suggested an interaction network centered on the electrostatic interactions at the dimer interface with long-range structural impacts. The crystal structures of SufS E96A and SufS E250A reported here show manipulation of interface electrostatic interactions does cause long-range structural changes to occur in the SufS dimer including a 3.5° rotation of monomer B versus monomer A (Figure 2C, 2D). The structures also show that the proposed link between the status of the R92-E250 salt bridge and the S254-C364 persulfide interaction does exist. The E96A and E250A SufS structures reveal a rotation of the β-hairpin structure away from the active site of monomer A, perhaps facilitating the C364 persulfide "out" conformation (Figure 2C, 2D, 3D). The extent of the conformational change is 2 Å located at S254. An interesting correlation was observed in the x-ray crystal structures: the E96A and E250A mutants, which had lower k_{cat}/K_{SufE} values, were also the mutants that possessed the long-range structural changes (Table 2, Figure 2C, 2D). When synthesized, these data indicate that the rotated-out β-hairpin must be a low affinity SufE state. At first this seems at odds with the fact that in the E96A and E250A mutants, C364 persulfide is pointed "out" poised for the transpersulfurase reaction. However, this can be reconciled if the rotated β-hairpin is considered to be a product complex, rather than a substrate complex, mimicking a state just after sulfur transfer to SufE. This state should necessarily have a weakened SufS-E interaction to promote SufE dissociation.

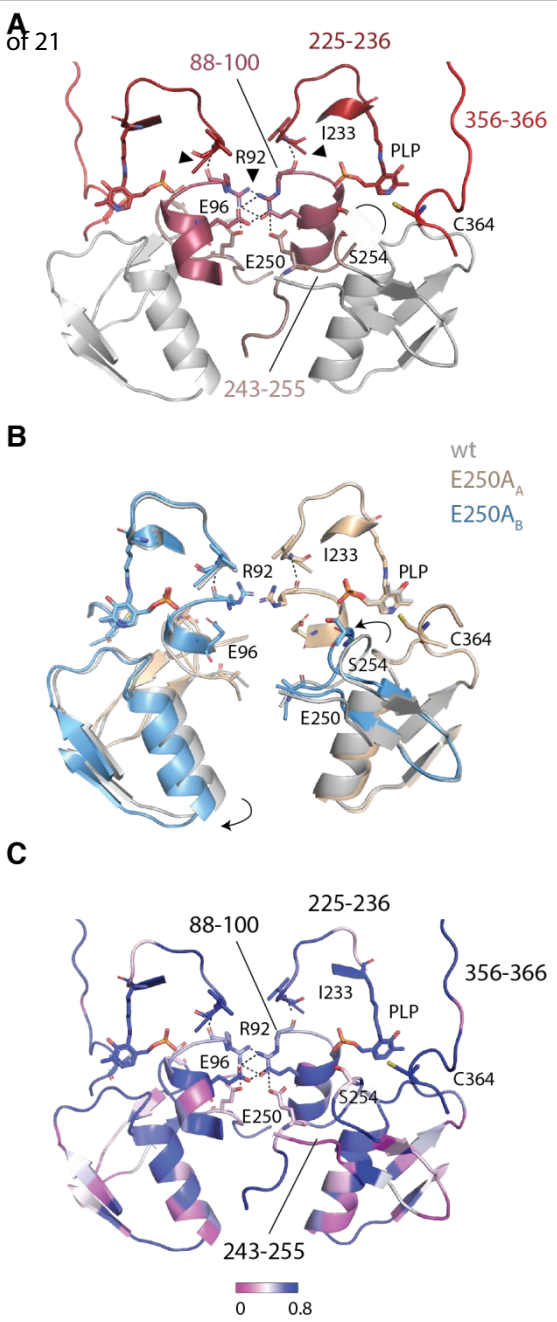

Figure 6. An interaction network centered on the dimer interface mediates crosstalk between the SufS active sites. (A) Peptides (shades of red) with altered dynamics in the C364 persulfide state are mapped onto the structure of the SufS dimer. (B) A superposition of wt SufS and E250A SufS indicates the conformational changes which occur when the network is broken. (C) Sequence conservation is mapped to the SufS structure to reveal that most components of the interaction network are conserved across SufS proteins.

While substantial conformational changes are observed for the two interface peptides identified by HDX-MS, 88-100 and 243-255, subtle changes are also observed for the active site peptides, 225-236 and 356-366 (Figure 6A, 5B). This includes the rotation of C364 persulfide into the "out" orientation in both the E96A and E250A structures and a subtle shift in the Lys226-PLP containing peptide (Figure 6B). The carbonyl of R92 hydrogen bonds to the amide of I233 providing a structural link between the dynamics of the 88-100 interface peptide and the 225-236 active site peptide (Figures 6A, 6B). The R92-I233 hydrogen bond is still present at 3.1 Å in the E250A structure, however in other structures along the reaction coordinate, not yet resolved, it could conceivably be lost. An additional piece of evidence that the R92 backbone interaction to I233 could be functionally significant comes from the fact that this region of peptide 225-236 is highly conserved (Figure 6C).

Evidence has previously been advanced that SufS enzymes use a half-sites mechanism in which one monomer participates in desulfurase chemistry while the adjacent monomer participates in transpersulfuration [14, 16]. This model requires SufS to form an asymmetric dimer and requires a mechanism for communication between the two active sites. The structures presented here and previous HDX-MS data have identified an interaction network composed of S254, the β-hairpin and the dimer interface that could plausibly serve as a conduit of communication between SufS active sites. SufS structures indicated active site residue H55 may also belong to the interaction network but kinetic assays disproved this hypothesis. The half-sites

model would be strengthened by the observation of an asymmetric SufS dimer. We did not observe an asymmetric arrangement of SufS likely because the crystals reported here did not contain SufE.

A half-sites regulatory mechanism fits with the proposed biological role of the SufS enzyme [33]. SufS is thought to promote Fe-S cluster synthesis under oxidative stress conditions because it is more resistant to oxidative stress than the alternative IscS-IscU pathway [17]. The inward facing conformation of C364 persulfide is expected to protect against oxidation and SufS rotates to the outward conformation, potentially exposing the persulfide to solvent, only just before reaction with SufE occurs. Understanding the mechanisms of SufS will clarify its biological role and by juxtaposition with other cysteine desulfurase mechanisms will improve understanding of diverse sulfur metabolism pathways.

ASSOCIATED CONTENT

Supporting Information

The following are included in Supporting Information: Figure S1 showing a size-exclusion chromatogram of the R92A, E96A and E250A SufS variants, Figure S2 showing a heat-map of atomic displacement parameters for the wild-type and E250A SufS structures, Figure S3 showing new interactions in SufS mutants at the dimer interface that drive dimer rearrangement, Figure S4 showing $F_o - F_c$ difference electron density in the vicinity of R92A, Figure S5 showing a heat-map of atomic displacement parameter values in the vicinity of C364 persulfide and Figure S6 showing a multiple sequence alignment of representative members of the SufS InterPro family IPR010970.

AUTHOR INFORMATION

Corresponding Authors

*Email: pfrantom@ua.edu; jadunkle@ua.edu

ORCID

Jack A. Dunkle 0000-0001-6252-0587

Patrick A. Frantom 0000-0001-7655-5967

Funding

This work was supported by NIH (GM112919). No competing financial interests have been declared.

ACKNOWLEDGMENT

We would like to thank Dr. Dokyong Kim for his assistance in purification of the SufS variants. Data were collected at Southeast Regional Collaborative Access Team (SER-CAT) 22-ID beamline at the Advanced Photon Source, Argonne National Laboratory. SER-CAT is supported by its member institutions (see www.ser-cat.org/members.html), and equipment grants (S10_RR25528 and S10_RR028976) from the National Institutes of Health. Use of the Advanced Photon Source was supported by the U. S. Department of Energy, Office of Science, Office of Basic Energy Sciences, under Contract No. W-31-109-Eng-38.

ABBREVIATIONS

wt, wild-type; EcSufS, E. coli SufS; PLP, 5'-pyridoxal-phosphate; HDX-MS, hydrogen-deuterium exchange mass spectrometry.

ACCESSION CODES

E. coli SufS (P77444)

The atomic coordinates and structure factors for SufS wt with an inward facing persulfide (6mr2), SufS H55A (6mr6), SufS R92A (6mre), SufS E96A (6mrh) and SufS E250A (6mri) have been deposited with the Protein Data Bank.

REFERENCES

[1] Ayala-Castro, C., Saini, A., and Outten, F. W. (2008) Fe-S cluster assembly pathways in bacteria, *Microbiol Mol Biol Rev 72*, 110-125, table of contents.

[2] Black, K. A., and Dos Santos, P. C. (2015) Shared-intermediates in the biosynthesis of thio-cofactors: Mechanism and functions of cysteine desulfurases and sulfur acceptors, *Biochim Biophys Acta 1853*, 1470-1480.

[3] Kim, D., Singh, H., Dai, Y., Dong, G., Busenlehner, L. S., Outten, F. W., and Frantom, P. A. (2018) Changes in Protein Dynamics in *Escherichia coli* SufS Reveal a Possible Conserved Regulatory Mechanism in Type II Cysteine Desulfurase Systems, *Biochemistry 57*, 5210-5217.

[4] Zheng, L., White, R. H., Cash, V. L., and Dean, D. R. (1994) Mechanism for the desulfurization of L-cysteine catalyzed by the nifS gene product, *Biochemistry 33*, 4714-4720.

[5] Tirupati, B., Vey, J. L., Drennan, C. L., and Bollinger, J. M., Jr. (2004) Kinetic and structural characterization of Slr0077/SufS, the essential cysteine desulfurase from *Synechocystis* sp. PCC 6803, *Biochemistry 43*, 12210-12219.

[6] Behshad, E., and Bollinger, J. M., Jr. (2009) Kinetic analysis of cysteine desulfurase CD0387 from *Synechocystis* sp. PCC 6803: formation of the persulfide intermediate, *Biochemistry 48*, 12014-12023.

[7] Mihara, H., Fujii, T., Kato, S., Kurihara, T., Hata, Y., and Esaki, N. (2002) Structure of external aldimine of *Escherichia coli* CsdB, an IscS/NifS homolog: implications for its specificity toward selenocysteine, *J Biochem 131*, 679-685.

[8] Kaiser, J. T., Clausen, T., Bourenkow, G. P., Bartunik, H. D., Steinbacher, S., and Huber, R. (2000) Crystal structure of a NifS-like protein from *Thermotoga maritima*: implications for iron sulphur cluster assembly, *J Mol Biol 297*, 451-464.

[9] Marinoni, E. N., de Oliveira, J. S., Nicolet, Y., Raulfs, E. C., Amara, P., Dean, D. R., and Fontecilla-Camps, J. C. (2012) (IscS-IscU)2 Complex Structures Provide Insights into Fe2S2 Biogenesis and Transfer, *Angewandte Chemie-International Edition 51*, 5439-5442.

[10] Prischi, F., Konarev, P. V., Iannuzzi, C., Pastore, C., Adinolfi, S., Martin, S. R., Svergun, D. I., and Pastore, A. (2010) Structural bases for the interaction of frataxin with the central components of iron-sulphur cluster assembly, *Nat Commun 1*, 95.

[11] Fujii, T., Maeda, M., Mihara, H., Kurihara, T., Esaki, N., and Hata, Y. (2000) Structure of a NifS homologue: X-ray structure analysis of CsdB, an *Escherichia coli* counterpart of mammalian selenocysteine lyase, *Biochemistry 39*, 1263-1273.

[12] Lima, C. D. (2002) Analysis of the E. coli NifS CsdB protein at 2.0 A reveals the structural basis for perselenide and persulfide intermediate formation, *J Mol Biol 315*, 1199-1208.

[13] Outten, F. W., Wood, M. J., Munoz, F. M., and Storz, G. (2003) The SufE protein and the SufBCD complex enhance SufS cysteine desulfurase activity as part of a sulfur transfer pathway for Fe-S cluster assembly in *Escherichia coli*, *J Biol Chem 278*, 45713-45719.

[14] Singh, H., Dai, Y., Outten, F. W., and Busenlehner, L. S. (2013) *Escherichia coli* SufE sulfur transfer protein modulates the SufS cysteine desulfurase through allosteric conformational dynamics, *J Biol Chem 288*, 36189-36200.

[15] Dai, Y., Kim, D., Dong, G., Busenlehner, L. S., Frantom, P. A., and Outten, F. W. (2015) SufE D74R Substitution Alters Active Site Loop Dynamics To Further Enhance SufE Interaction with the SufS Cysteine Desulfurase, *Biochemistry 54*, 4824-4833.

[16] Selbach, B., Earles, E., and Dos Santos, P. C. (2010) Kinetic analysis of the bisubstrate cysteine desulfurase SufS from *Bacillus subtilis*, *Biochemistry 49*, 8794-8802.
[17] Dai, Y., and Outten, F. W. (2012) The E. coli SufS-SufE sulfur transfer system is more resistant to oxidative stress than IscS-IscU, *FEBS Lett 586*, 4016-4022.
[18] Selbach, B. P., Pradhan, P. K., and Dos Santos, P. C. (2013) Protected sulfur transfer reactions by the *Escherichia coli* Suf system, *Biochemistry 52*, 4089-4096.
[19] Kabsch, W. (2014) Processing of X-ray snapshots from crystals in random orientations, *Acta Crystallogr D Biol Crystallogr 70*, 2204-2216.
[20] Otwinowski, Z., and Minor, W. (1997) Processing of X-ray diffraction data collected in oscillation mode, *Methods Enzymol 276*, 307-326.
[21] Adams, P. D., Afonine, P. V., Bunkoczi, G., Chen, V. B., Davis, I. W., Echols, N., Headd, J. J., Hung, L. W., Kapral, G. J., Grosse-Kunstleve, R. W., McCoy, A. J., Moriarty, N. W., Oeffner, R., Read, R. J., Richardson, D. C., Richardson, J. S., Terwilliger, T. C., and Zwart, P. H. (2010) PHENIX: a comprehensive Python-based system for macromolecular structure solution, *Acta Crystallogr D Biol Crystallogr 66*, 213-221.
[22] Emsley, P., Lohkamp, B., Scott, W. G., and Cowtan, K. (2010) Features and development of Coot, *Acta Crystallogr D Biol Crystallogr 66*, 486-501.
[23] Schrodinger, LLC. (2015) The PyMOL Molecular Graphics System, Version 1.8.
[24] Weinert, T., Olieric, V., Waltersperger, S., Panepucci, E., Chen, L., Zhang, H., Zhou, D., Rose, J., Ebihara, A., Kuramitsu, S., Li, D., Howe, N., Schnapp, G., Pautsch, A., Bargsten, K., Prota, A. E., Surana, P., Kottur, J., Nair, D. T., Basilico, F., Cecatiello, V., Pasqualato, S., Boland, A., Weichenrieder, O., Wang, B. C., Steinmetz, M. O., Caffrey, M., and Wang, M. (2015) Fast native-SAD phasing for routine macromolecular structure determination, *Nat Methods 12*, 131-133.
[25] Liu, Q., Dahmane, T., Zhang, Z., Assur, Z., Brasch, J., Shapiro, L., Mancia, F., and Hendrickson, W. A. (2012) Structures from anomalous diffraction of native biological macromolecules, *Science 336*, 1033-1037.
[26] Karplus, P. A., and Diederichs, K. (2012) Linking crystallographic model and data quality, *Science 336*, 1030-1033.
[27] Atkinson, H. J., Morris, J. H., Ferrin, T. E., and Babbitt, P. C. (2009) Using sequence similarity networks for visualization of relationships across diverse protein superfamilies, *PLoS One 4*, e4345.
[28] Shannon, P., Markiel, A., Ozier, O., Baliga, N. S., Wang, J. T., Ramage, D., Amin, N., Schwikowski, B., and Ideker, T. (2003) Cytoscape: a software environment for integrated models of biomolecular interaction networks, *Genome Res 13*, 2498-2504.
[29] Gerlt, J. A., Bouvier, J. T., Davidson, D. B., Imker, H. J., Sadkhin, B., Slater, D. R., and Whalen, K. L. (2015) Enzyme Function Initiative-Enzyme Similarity Tool (EFI-EST): A web tool for generating protein sequence similarity networks, *Biochim Biophys Acta 1854*, 1019-1037.
[30] Edgar, R. C. (2004) MUSCLE: multiple sequence alignment with high accuracy and high throughput, *Nucleic Acids Res 32*, 1792-1797.
[31] Ritter, B., Denisov, A. Y., Philie, J., Deprez, C., Tung, E. C., Gehring, K., and McPherson, P. S. (2004) Two WXXF-based motifs in NECAPs define the specificity of accessory protein binding to AP-1 and AP-2, *EMBO J 23*, 3701-3710.
[32] Kim, S., and Park, S. (2013) Structural changes during cysteine desulfurase CsdA and sulfur acceptor CsdE interactions provide insight into the trans-persulfuration, *J Biol Chem 288*, 27172-27180.
[33] Boyd, E. S., Thomas, K. M., Dai, Y., Boyd, J. M., and Outten, F. W. (2014) Interplay between oxygen and Fe-S cluster biogenesis: insights from the Suf pathway, *Biochemistry 53*, 5834-5847.

Table of Contents Graphic.